Spectroscopic and crystal field studies of Nd^{3+} in $GdCa_4O(BO_3)_3$ and $YCa_4O(BO_3)_3$

A. Lupei
Institute of Atomic Physics, Bucharest, MG 76900, Romania

E. Antic-Fidancev, G. Aka, D. Vivien, and P. Aschehoug
Laboratoire de Chimie Appliquée de l'Etat Solide, CNRS UMR 7574, ENSCP, 11, rue Pierre et Marie Curie, F-75231 Paris, France

Ph. Goldner and F. Pellé
Groupe d'Optique des Terres Rares, CNRS UMR 7574, F-92195 Meudon-Bellevue, France

L. Gheorghe
Institute of Atomic Physics, Bucharest, MG 76900, Romania

(Received 22 May 2001; revised manuscript received 13 February 2002; published 11 June 2002)

The calcium rare-earth oxoborate crystals $RCa_4O(BO_3)_3$-RCOB with R^{3+} as Gd^{3+} or Y^{3+} represent promising laser and nonlinear materials for the development of compact near IR and visible laser sources. New results on Nd^{3+} spectral characteristics in GdCOB and YCOB crystals in connection to the crystal structure are presented. Low-temperature absorption and selectively excited emission spectra of Nd^{3+} in RCOB crystals, grown by the Czochralski method in iridium crucible, present one prevailing center corresponding to Nd^{3+} ions in the R^{3+} site of C_s symmetry and at least three minority centers. Crystal field modeling gives a set of free ion and crystal field parameters that describe well the experimentally obtained energy level schemes for the main centers. A comparison between the Nd^{3+} crystal field splittings in RCOB and those of the C_2 site in C-type Y_2O_3 in terms of rare-earth environments is made. The selectively excited emission, lifetimes, and structural data were used to elucidate the nature of the minority centers. Two of the them were associated with Nd^{3+} in R^{3+} sites slightly perturbed by charged intrinsic lattice defects of nonstoichiometric or inversion Gd^{3+} $(Y^{3+})\leftrightarrow Ca^{2+}$ type, while the third Nd^{3+} center is assigned to Nd^{3+} in a Ca^{2+} site. Other features of the spectra such as vibronics or homogeneous linewidths are also discussed. The Gaussian line shape and main contributions to inhomogeneous broadening are analyzed. An additional source of broadening for Nd^{3+} in YCOB is revealed.

DOI: 10.1103/PhysRevB.65.224518 PACS number(s): 78.55.Kz, 42.55.Rz, 42.70.Hj

I. INTRODUCTION

During the last years a new class of Nd^{3+} doped nonlinear crystals has been developed, calcium rare-earth oxoborates, $RCa_4O(BO_3)_3$-RCOB, with special attention to GdCOB and YCOB. These crystals possess properties that make them present among the most studied laser and nonlinear materials.[1–24] Good optical quality crystals of large dimensions could be grown by Czochralski (or Bridgman) techniques. They are efficient nonlinear optical materials, with large transparency range, high damage threshold, and nonhygroscopicity. Doped with Nd^{3+} they can be used as self-frequency-conversion crystals, which combine laser and nonlinear properties for intracavity transformation of the fundamental infrared laser wavelength into blue, green, or red emission. Diode pumping is also favored by the fairly good absorption of Nd^{3+} ions in the region of high power near infrared laser diodes.[20–22] Such crystals are promising materials to develop diode-pumped visible microchip lasers for alignment, pointing, or medical applications.

Most of the published papers on $RCa_4O(BO_3)_3$ doped with Nd^{3+} refer to crystal growth, nonlinear characteristics, laser emission in the 1-μm range in various regimes, doubling, or self-frequency multiplication.[6–22] No detailed low-temperature spectroscopic data for Nd^{3+} in RCOB have been published up to now. Thus, no extended energy level scheme has been reported, except for the levels involved in the laser process at the fundamental emission frequency, or crystal field calculations. The use of Nd^{3+}:RCOB as self-frequency-conversion crystals requires knowledge of whole energy level diagrams.

The RCOB crystals are monoclinic with a single position of C_s symmetry[2] for R^{3+} ions, while Ca^{2+} ions occupy two sites of C_1 symmetry, $Ca^{2+}(1)$ and $Ca^{2+}(2)$. Nd^{3+} ions could enter in any of the three cationic sites. The Nd^{3+} optical spectra have revealed[7] in GdCOB the presence of a prevailing center associated with Nd^{3+} in the R^{3+} site and several satellites. Several structural models can account for these satellites such as occupation of other cationic sites (Ca^{2+}), Nd^{3+} in R^{3+} positions perturbed by the presence in a near lattice site of another dopant ion or of a structural defect. A detailed investigation of the spectral characteristics of satellites lines, not performed up to now, can allow elucidation of their nature. The main lattice defects in RCOB pure crystals are associated with structural disorder.[1,2,7,9,12,22] The actual structural model for RCOB, the degree of disorder, and its dependence on R^{3+} or on the type and concentration of the dopant ion has not yet been clarified.

The purpose of this paper is to analyze the low-temperature Nd^{3+} optical spectra characteristics in GdCOB and YCOB crystals, to obtain energy level schemes, to perform crystal field calculations for the prevailing centers, and

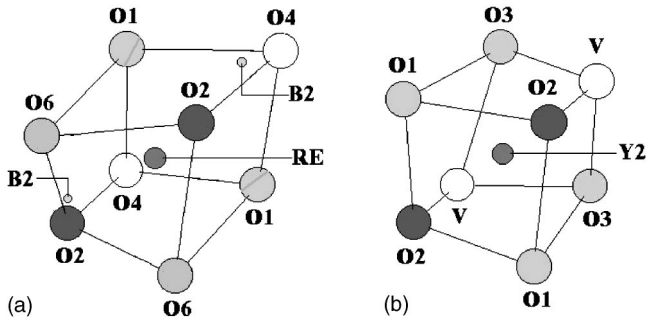

FIG. 1. (a) The first near neighbor of R^{3+} in RCOB and (b) the similar environment for Nd^{3+} in Y_2O_3; V are oxygen vacancies.

to bring new data by selective excitation in order to clarify the nature of nonequivalent centers and structural disorder. In Sec. II some details of RCOB structure are given, and in Sec. III the experimental setup is briefly described. Section IV is dedicated to a description of the low-temperature absorption and selective excited emission spectra, as well as emission kinetics. The results of the crystal field calculation for the Nd^{3+} prevailing center in GdCOB are presented in Sec. V. An analysis of the static crystal field effects, the coupling with lattice vibrations, nonequivalent centers, and inhomogeneous broadening is presented in Sec. VI and several conclusions are stated.

II. STRUCTURAL CONSIDERATIONS

In order to analyze the optical spectra features some local structural details for cationic sites in RCOB were obtained by using a computer program Carinev3 and x-ray data.[2] The space group of RCOB crystals is monoclinic, noncentrosymmetric Cm. The unit cell parameters for GdCOB are $a = 8.078$ Å, $b = 15.98$ Å, $c = 3.55$ Å, $\beta = 101.28°$, and slightly different for YCOB.[2] The RCOB structure contains a unique rare-earth site, two types of Ca^{2+} sites [$Ca^{2+}(1)$ and $Ca^{2+}(2)$], and two distinct $(BO_3)^{3-}$ groups [B(1) and B(2)]. The R^{3+} ions occupy a site of C_s symmetry[2] with six close oxygen ions, and other two O^{2-} at larger distances, with two $B^{3+}(2)$ ions intercalated. The R^{3+} ions are situated in a mirror plane on a chain along the c axis at distances around 3.55 Å and the distances between chains are more than double. The density of R^{3+} sites in RCOB is rather small, $\sim 4.5\times 10^{21}$ ions/cm^3. The R^{3+} environment is given in Fig. 1(a) and in Table I the Gd^{3+} near-neighbor distances in GdCOB are given (the notation of Norrestam *et al.*[2] is used). A similarity between the R^{3+} environment in RCOB and Y^{3+} main site[25] in Y_2O_3 is observed. Thus, if in RCOB the R^{3+} has an eightfold coordination with two O^{2-} at much larger distances [Fig. 1(a)], the Y^{3+} main site in C-type Y_2O_3 is an eightfold coordination with two oxygen vacancies (V) on a face diagonal and possesses C_2 symmetry [Fig. 1(b)]; the distances from near neighbors to Y^{3+} are also given in Table I. Ca^{2+} ions enter in two sites of C_1 symmetry, $Ca^{2+}(1)$ in a sixfold O^{2-} coordination and $Ca^{2+}(2)$ in an eightfold distorted O^{2-} coordination, and two $B^{3+}(2)$ ions are intercalated between the first six O^{2-} and the other two; the $Ca^{2+}(2)$ near-neighbors positions in GdCOB are also given in Table I. Thus, the R^{3+} surrounding looks closer to that of $Ca^{2+}(2)$, rather than that of $Ca^{2+}(1)$.

According to the ionic radii,[26] Nd^{3+} ions could occupy any of the three cationic sites: R^{3+}, $Ca^{2+}(1)$, and $Ca^{2+}(2)$. The preference of Nd^{3+} for R^{3+} was outlined previously,[7] but the occupancy of Ca^{2+} sites has not been clearly established. From the first published papers on the RCOB structure,[1,2] the existence of some disorder in the occupancy of R^{3+} and Ca^{2+} sites was outlined; the disorder increases with decreasing R^{3+} ionic radii. Subsequent studies[7,9] on GdCOB crystals grown in iridium in nitrogen atmosphere have also remarked on the presence of some disorder in these crystals. Y^{3+} excess as compared with Ca^{2+} was measured[12] for crystals grown in iridium Nd^{3+}:YCOB crystals, while more recently,[22] good quality pure YCOB crystals with Ca^{2+} excess were reported. Ionic vacancies could also appear in these crystals.[24] The spectroscopic study[27] of Yb^{3+} in GdCOB and YCOB has revealed a much larger disorder in the later case. This difference is supported by the presence of several peaks in the differential thermal analysis (DTA) cooling curve[28] for YCOB compared with a single-peak GdCOB.

TABLE I. R^{3+} and $Ca^{2+}(2)$ environment in GdCOB and Y_2O_3.

Gd^{3+} near-neighbor distances[a] (Å) in GdCOB		Ca^{2+} (2) near-neighbor distances[a] (Å) in GdCOB		Y^{3+} near-neighbor distances[b] (Å) in Y_2O_3	
Gd-O(1)	2.2438	Ca(2)-O(2)	2.3277	Y(2)-O(2)	2.2487
Gd-O(1)	2.2578	Ca(2)-O(2)	2.3362	Y(2)-O(2)	2.2487
Gd-O(2)	2.4206	Ca(2)-O(5)	2.3397	Y(2)-O(3)	2.2784
Gd-O(2)	2.4206	Ca(2)-O(3)	2.4621	Y(2)-O(3)	2.2784
Gd-O(6)	2.3660	Ca(2)-O(4)	2.4956	Y(2)-V	2.3296
Gd-O(6)	2.4519	Ca(2)-O(3)	2.6169	Y(2)-V	2.3296
Gd-B(2)	3.1670	Ca(2)-B(2)	2.7652	Y(2)-O(1)	2.3358
Gd-B(2)	3.1670	Ca(2)-O(3)	2.8707	Y(2)-O(1)	2.3358
Gd-O(4)	3.1914	Ca(2)-B(2)	2.9328		
Gd-O(4)	3.1914	Ca(2)-O(6)	2.9506		

[a]Reference 2.
[b]Reference 25.

Any of the discussed possibilities—occupation of Ca^{2+} sites, pairs or structural defects close to Nd^{3+} ions—imply that they are submitted to different crystal fields that could determine satellite lines in the optical spectra or contribute to inhomogeneous broadening.

III. EXPERIMENT

The high-quality crystals were grown by the Czochralski method in iridium crucible under nitrogen atmosphere, with actual Nd^{3+} content from 4 to 7 at. %, as used in laser experiments. Some samples were grown in platinum crucibles too. The low-temperature absorption spectra were recorded on different polarizations from far infrared to UV by using a Cary 5 Varian spectrophotometer; oriented samples were studied. The low-temperature emission spectra as well as selective excitation were obtained with a cw Ti:sapphire laser (Coherent 890) pumped with an argon ion laser. The spectra were analyzed with an ARC SpectraPro-7510 monochromator and detected with a cooled InGaAs photodiode. Lifetimes were recorded using a pulsed (10 ns) Ti:sapphire laser (BMI TS 802) pumped by a frequency-doubled YAG: Nd laser (BMI 501 DNS 720). The fluorescence was dispersed by a HD 460 Jobin-Yvon monochromator and detected by a nitrogen-cooled InAs photodiode (1 μs time constant).

IV. SPECTROSCOPIC MEASUREMENTS

The Nd^{3+} low-temperature optical spectra are very similar in GdCOB and YCOB crystals. In the following paragraphs the spectral features of Nd^{3+} in GdCOB shall be described in detail, while the differences for YCOB shall be only mentioned.

A. Absorption spectra

The absorption spectra were recorded from 250 to 2500 nm at 10 K. In the case of GdCOB part of the UV Nd^{3+} lines (in the 250–370 nm region) interfere with those of Gd^{3+} ions. The local symmetry at the Nd^{3+} ion is C_s or lower, so that all levels are Kramers doublets. Spectra are strongly dependent on polarization. The samples were oriented along the optical axes (X, Y, Z), which are related to crystallographic ones (a, b, c) as $b \| Y$, $(a,Z)=26°$, $(c,X)=15°$ for GdCOB and $b \| Y$, $(a,Z)=24.7°$, $(c,X)=13.5°$ for YCOB. Since in the case of Nd^{3+} lasers, the $E||Z$ polarization is important for self-frequency doubling, we have restricted the low-temperature measurements to two polarizations $E||X$ and $E||Z$. Figure 2 presents the $^4I_{9/2} \rightarrow {}^4F_{3/2}$ absorption spectrum of a GdCOB sample doped with 7 at. % Nd^{3+} at 10 K for these two polarizations. Besides the lines corresponding to transitions to two Stark components of the $^4F_{3/2}$ main center (MC), R_1 and R_2, the presence of two satellites (C_i) of dissimilar intensity situated at -41 and $+46$ cm^{-1} from the R_1 line corresponding to the $^4I_{9/2}(1) \rightarrow {}^4F_{3/2}(1)$ transition is evidenced [(1) denoting the lowest Stark level of the manifold]. The relative intensity of the $C_{2,3}$ satellite (at -41 cm^{-1}) to the total intensity is ~3%–4% and is, in the limit of experimental errors, the same for all the investigated

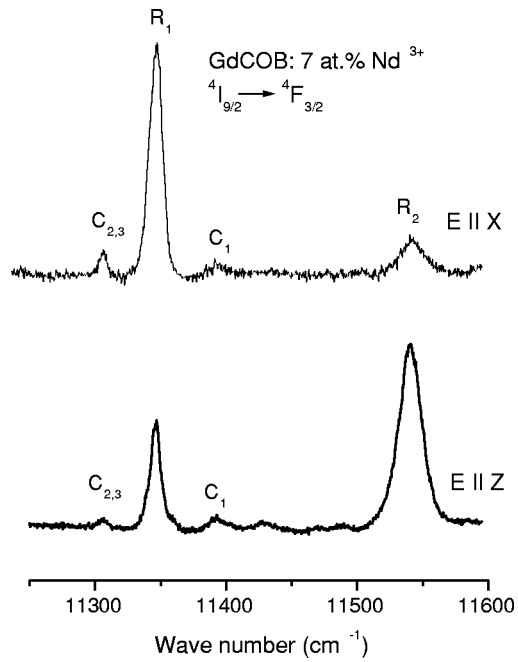

FIG. 2. Absorption spectra of Nd^{3+} (7 at. %) at 10 K in GdCOB corresponding to the $^4I_{9/2}(1) \rightarrow {}^4F_{3/2}$ transition in two polarizations; C_i denote perturbed center lines.

Nd^{3+} concentrations. The relative intensity of the C_1 line (at $+46$ cm^{-1}) is ~2%–3%. The lowest electronic line (the diode pumping line) of the absorption spectrum associated with the $^4I_{9/2} \rightarrow {}^4F_{5/2} + {}^2H_{9/2}$ transitions (Fig. 3) of Nd^{3+} in GdCOB is also surrounded by two satellites of unequal intensity. Similar structures are observed for Nd^{3+} in YCOB, but the lines are much broader.

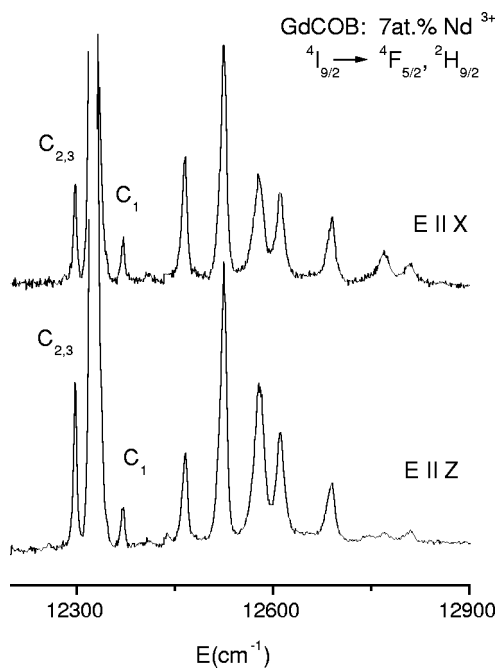

FIG. 3. Polarization effects in the $^4I_{9/2}(1) \rightarrow {}^4F_{5/2}$, $^2H_{9/2}$ transition of Nd^{3+} in GdCOB at 10 K; C_i are perturbed center lines.

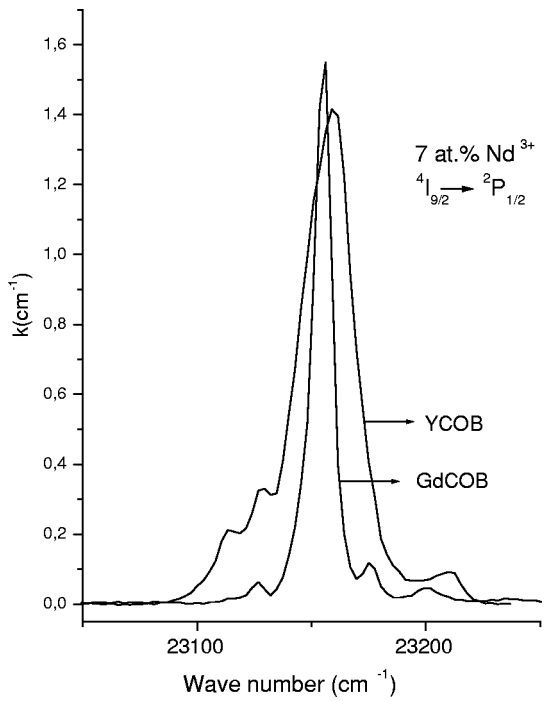

FIG. 4. Satellite structure of Nd^{3+} (7 at.%) in GdCOB and YCOB as observed in the $^4I_{9/2}(1)\rightarrow{}^2P_{1/2}$ transition at 10 K.

An appropriate transition for the study of different environments of Nd^{3+} ion is $^4I_{9/2}\rightarrow{}^2P_{1/2}$. For Nd^{3+} in GdCOB one could observe in this transition (Fig. 4) three satellite lines with similar intensities situated at -29, $+19$ and $+43$ cm^{-1} from the main line. For Nd^{3+} in YCOB (Fig. 4) for the same concentration (7 at.%), the MC linewidth is significantly larger and the satellite structure is different. This three-line satellite structure seems to be in discrepancy with only two satellites in the spectra corresponding to $^4I_{9/2}(1)\rightarrow{}^4F_{3/2}(1)$ (Fig. 2) or $^4I_{9/2}\rightarrow{}^4F_{5/2}(1)$ transitions (Fig. 3). However, as we shall show later, this fact is due to an accidental degeneracy. The inhomogeneous broadening and its dependence on the crystal and Nd^{3+} concentration shall be analyzed in Sec. VII.

Other features of the low-temperature Nd^{3+} spectra in GdCOB and YCOB are the phonon sidebands and large homogeneous broadening of many zero-phonon lines. These crystals present rich phonon spectra, as observed by Raman[29,30] and IR (Ref. 7) techniques. The electron-phonon coupling manifests in rather strong vibronics for Nd^{3+} ion, especially in $^4I_{9/2}\rightarrow(^4G_{5/2},\ ^2G_{7/2})$, $(^4G_{7/2},\ ^2K_{13/2}$, and $^4G_{9/2})$, and $(^2G(1)_{9/2},{}^2D(1)_{3/2},{}^4G_{11/2},{}^2K_{15/2})$ transitions. In order to separate zero-phonon lines from vibronics an analysis of the spectra similar to that performed previously,[31] by using Raman and IR data, was undertaken.

B. Emission spectra under selective excitation and lifetimes

The emission spectra corresponding to $^4F_{3/2}(1)\rightarrow{}^4I_J$ transitions (with $J=9/2$, 11/2, 13/2) under selective excitation were obtained by pumping in the region of the $^4I_{9/2}(1)\rightarrow{}^4F_{5/2}(1)$ transition. Figure 5 presents the emission spectra of Nd^{3+} in GdCOB associated with $^4F_{3/2}(1)$

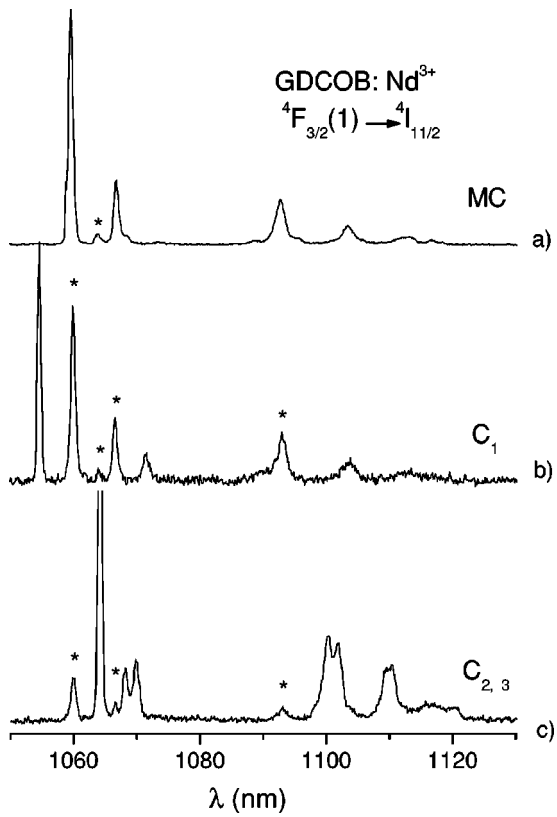

FIG. 5. Emission spectra corresponding to $^4F_{3/2}(1)\rightarrow{}^4I_{11/2}$ transitions under selective pumping in $^4I_{9/2}(1)\rightarrow{}^4F_{5/2}$ at 10 K; ⋆ denotes the lines associated with the nonselective excitation of other center (MC or $C_{2,3}$) emissions.

$\rightarrow{}^4I_{11/2}$ transitions for pumping in MC and C_i centers. Some of the lines in Fig. 5 (denoted by an asterisk) correspond to other excited center (MC or $C_{2,3}$) emissions. One could see in the emission spectra [Fig. 5(c)] the doubling of some lines, the splittings (up to 10 cm^{-1}) depending on the transition. The same behavior is observed in other transitions too. This means that in $^4I_{9/2}(1)\rightarrow{}^4F_{3/2}(1)$ and $^4F_{5/2}(1)$ transitions we have an accidental degeneracy between C_2 and C_3 centers lines. The energy level scheme of the Nd^{3+}-$^4I_{9/2}$ manifold in GdCOB, presented in Fig. 6, is a suggestive illustration. Therefore, at least four different Nd^{3+} environments exist in GdCOB. The energy level schemes (Fig. 6), as well as the spectra presented in Figs. 4 and 5, show that two of the perturbed Nd^{3+} sites $C_{2,3}$ in GdCOB present very close optical spectra and similar to those of the MC. It is difficult to obtain energy levels for the entire range of C_i centers; therefore, only the energy level schemes of the MC are given in Table II. The energy levels of the lowest manifolds for the C_1 center in YCOB are almost identical to those in GdCOB, but slight differences are observed for $C_{2,3}$ centers, the lines being so much larger that they cannot be separated.

The Nd^{3+} MC lines in YCOB at the same concentration present a higher inhomogeneous broadening. The selective excitation in main lines leads to several emission wavelengths, a behavior characteristic to crystals with disordered structure. Figure 7(a) shows the $^4I_{9/2}(1)\rightarrow F_{5/2}(1)$ excita-

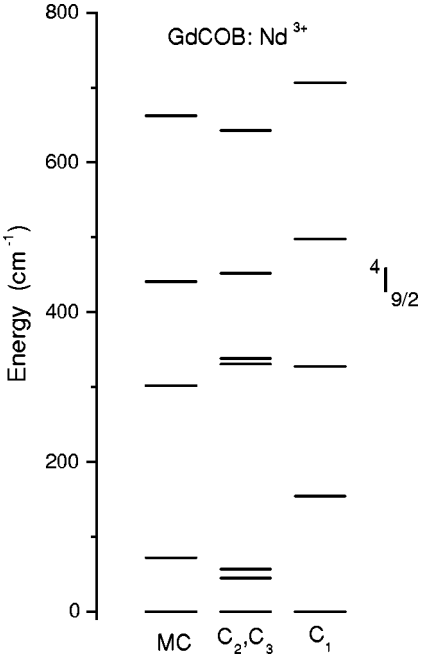

FIG. 6. Crystal field splittings of the Nd^{3+} $^4I_{9/2}$ level in GdCOB for the MC and perturbed C_i centers.

tion spectra obtained by monitoring slightly different wavelengths inside MC $^4F_{3/2}(1)\rightarrow I_{11/2}(1)$ emission. A broadband analysis reveals in the MC line two main peaks which can be resolved with a more selective analysis. Since we choose the selective analysis wavelength randomly, it is very likely that the main line inhomogeneous broadening is due to a quasicontinuous distribution of sites.

$^4F_{3/2}$ decay curves were measured at 10 K with 1 μs resolution by monitoring the $^4F_{3/2}(1)\rightarrow{}^4I_{11/2}(1)$ transition for the three centers in Nd 4 at.%:GdCOB. All decays were exponential with similar lifetimes: MC, 95 μs; C_1, 91 μs, $C_{2,3}$, 92 μs. The lifetime obtained for the MC is close to that reported at 300 K in GdCOB at low Nd^{3+} concentrations[7] (98 μs). This indicates that MC $^4F_{3/2}$ level emission is not affected by energy transfer at low temperature. C_i center lifetimes are only slightly smaller than the MC one. This last result suggests that C_i sites do not correspond to pairs or clusters in which the energy transfer would strongly decrease the lifetimes.

The $^4F_{3/2}$ lifetimes in Nd^{3+} (7 at.%): YCOB (MC, 95 μs; C_1, 85 μs, $C_{2,3}$, 88 μs) are similar to those recorded in Nd^{3+} 4 at.%:GdCOB. Since Nd^{3+} concentrations were significantly different in the samples, this result is also in agreement with a negligible energy transfer between MC sites at low temperature. C_i centers have also only slightly smaller lifetimes than the MC, without any evidence of the strong interactions which should be found in pairs or larger aggregates. Once more we noticed that no migration of energy occurs inside the main line as shown by the emission spectra obtained at different excitation wavelengths [Fig. 7(b)].

V. CRYSTAL FIELD CALCULATION

Based on absorption and emission spectra and their analysis, experimental energy level diagrams of Nd^{3+} in GdCOB and YCOB were established in the range 0–40 000 cm^{-1} (Table II). The crystal field simulation was performed considering 182×182 Kramers doublets of the $4f^3$ configuration. The perturbation contains the free ion and crystal field interactions. The free ion Hamiltonian $\hat{H}_{FI}$ can be written as

$$\hat{H}_{FI}=\hat{H}_0+\sum_{k=0}^{3}\hat{e}_k E^K+\varsigma_{4f}\hat{A}_{SO}+\alpha\hat{L}(\hat{L}+1)+\beta\hat{G}(G_2)+\gamma\hat{G}(R_7)+\sum_{\lambda=2}^{8\neq 5}\hat{t}_\lambda T_\lambda,$$

where $\hat{H}_0$ is the spherically symmetric one-electron term of the Hamiltonian, E^k and ζ_{4f} are the Racah parameters and the spin-orbit coupling constant, and $\hat{e}_k$ and $\hat{A}_{SO}$ represent the angular parts of the electrostatic repulsion and spin-orbit coupling, respectively. For $4f^N$ configurations with $N>2$ two-body interactions have to be considered with Trees' α, β, and γ parameters associated with $\hat{L}$, total angular momentum operator, and $\hat{G}(G_2)$ and $\hat{G}(R_7)$ Casimir operators. For configurations with $N>2$ three-body interactions with Judd T^λ (T^2, T^3, T^4, T^6, T^7, T^8) parameters are of importance. $\hat{t}_\lambda$ are operators transforming according to the irreducible groups G_2 and R_7.

The perturbation due to crystalline field depending on the local symmetry around the R^{3+} ion can be described in the frame of the Wybourne formalism.[32] The local environment for the Nd^{3+} MC in both investigated compounds is C_s, which requires 15 crystal field parameters. The crystal field Hamiltonian is written as

$$\hat{H}_{CF}(C_s)=\sum_k B_0^k\hat{C}_0^k+\sum_{k,q>0}B_q^k[\hat{C}_q^k+\hat{C}_{-q}^k]+iS_q^k[\hat{C}_q^k-\hat{C}_{-q}^k],$$

with $k=2,4,6$ and $q\leqslant k$, $\hat{C}_q^k$ are spherical operators of rank k and order q, and B_q^k and S_q^k represent crystal field splitting parameters.

In the crystal field phenomenological procedure 95 Stark levels of the Nd^{3+} prevailing center in GdCOB were used up to the $^4D_{1/2}$ level situated in the UV. Free ion and crystal field parameters were refined by means of the IMAGE program.[33] The starting sets of free ion parameters and crystal field parameters were taken from previous calculations[34–36] on systems with similar energy level schemes. As in these cases we considered only 14 phenomenological crystal field parameters, S_2^2 being canceled by a proper choice of reference axis system. The best-fit parameter set is listed in Table III. The final root-mean-square deviation, taken as a figure of merit, is 17.7 cm^{-1}. This result is reasonable taking into account the complexity of the problem. Some of the high UV levels are not clearly identified, so the levels above 28 500 cm^{-1} $^4D_{1/2}$) were not used in the fit. However, a series of levels around 34 000 cm^{-1} is well fitted, which gives us confidence in the set of crystal field parameters. Experimental and calculated $^2H_{11/2}$ Stark sub-

TABLE II. Energy levels of Nd^{3+} in $GdCa_4O(BO_3)_3$ (experimental and calculated) and in $YCa_4O(BO_3)_3$ (experimental).

$^{2S+1}L_J$ levels	GdCOB Energy expt. (cm^{-1})	GdCOB Energy calc. (cm^{-1})	YCOB Energy expt. (cm^{-1})	$^{2S+1}L_J$ levels	GdCOB Energy expt. (cm^{-1})	GdCOB Energy calc. (cm^{-1})	YCOB Energy expt. (cm^{-1})
$^4I_{9/2}$	0	−8	0	$^2H(2)_{11/2}$	15 827	-	15 836
	74	81	73		15 868	-	15 877
	304	316	300		15 900	-	15 905
	452	457	451		16 026	-	16 024
	670	673	680		16 091	-	16 091
					16 126	-	16 130
$^4I_{11/2}$	1909	1922	1908				
	1974	1962	1975	$^4G_{5/2}$	16 811	16 824	16 826
	2196	2174	2195		16 975	17 003	16 983
	2284	2271	2281	+	17 083	17 095	17 092
	2357	2345	2356	$^2G_{7/2}$	17 206	17 226	17 219
	2393	2390	2407		17 301	17 281	17 307
					17 388	17 381	17 391
$^4I_{13/2}$	3832	3849	3833		17 526	17 512	17 530
	3889	3874	3889				
	4152	4127	4148	$^4G_{7/2}$	18 678	18 687	18 697
	4222	4211	4222		18 796	18 805	18 811
	4270	4301	4323	+	18 921	18 909	18 912
	4325	4325	4337		18 961	18 948	18 970
	4374	4381	4380	$^2K_{13/2}$	19 011	18 998	19 011
				+	19 307	19 304	19 320
$^4I_{15/2}$	5724	5736	5726	$^4G_{9/2}$	19 381	19 390	19 395
	5798	5810	5798		19 436	19 435	19 447
	6119	6111	6116		19 469	19 455	19 474
	6193	6204	6183		19 496	19 498	19 503
	6404	6392	6405		19 542	19 542	19 546
	6438	6442	6440		19 646	19 630	19 658
	6478	6493	6486		-	19 764	-
	6538	6537	-		19 859	19 851	19 861
					19 954	19 967	20 040
$^4F_{3/2}$	11 346	11 340	11 347		20 129	20 131	20 153
	11 539	11 506	11 537				
				$^2G(1)_{9/2}$	20 680	20 659	20 691
$^4F_{5/2}$	12 328	12 314	12 326		20 715	20 696	20 734
	12 466	12 464	12 472	+	20 823	20 811	20 831
	12 526	12 510	12 524	$^2D(1)_{3/2}$	20 913	20 911	20 914
+	12 579	12 585	12 581		20 968	20 968	20 966
	12 613	12 622	12 612	+	21 035	21 039	21 035
$^2H(2)_{9/2}$	12 690	12 664	12 681		-	21 063	21 090
	12 772	12 815	12 782	$^4G_{11/2}$	21 138	21 157	21 143
	12 809	12 844	12 807		21 222	21 209	21 229
				+	21 294	21 301	21 295
$^4F_{7/2}$	13 342	13 356	13 333		21 366	21 369	-
+	13 443	13 469	13 450		-	21 440	-
	13 521	13 527	13 517	$^2K_{15/2}$	21 566	21 545	-
$^4S_{3/2}$	13 551	13 544	13 554		21 696	21 688	21 708
	13 652	13 663	13 665		-	21 728	-
					21 770	21 782	-
$^4F_{9/2}$	14 570	14 593	14 575		21 848	21 870	22 104
	14 667	14 672	14 667		21 918	21 940	-
	14 728	14 710	14 721		21 981	21 967	21 959
	14 876	14 867	14 865		221 74	22 147	22 195
	15 011	15 000	-				

TABLE II. *(Continued).*

$^{2S+1}L_J$ levels	GdCOB Energy expt. (cm^{-1})	GdCOB Energy calc. (cm^{-1})	YCOB Energy expt. (cm^{-1})	$^{2S+1}L_J$ levels	GdCOB Energy expt. (cm^{-1})	GdCOB Energy calc. (cm^{-1})	YCOB Energy expt. (cm^{-1})
$^2P_{1/2}$	23 154	23 152	23 159		30 679	30 671	30 656
					-	30 760	-
$^2D(1)_{5/2}$	23 566	23 579	23 585		30 838	30 830	-
	23 746	23 740	-				
	-	23 980	-	$^2L_{17/2}$	-	30 886	30 873
$^2P_{3/2}$	25 965	25 950	25 966		-	31 118	-
	26 158	26 150	26 169		-	31 476	-
						31 586	
$^4D_{3/2}$	27 632	27 619	27 624		-	31 729	-
+	27 709	27 686	27 716		-	31 880	-
$^4D_{5/2}$	27 806	27 795	27 801		-	32 000	-
	28 130	28 147	28 169		-	32 175	-
	28 341	28 347	28 353		-	32 284	-
					-	32 478	-
$^4D_{1/2}$	28 493	28 520	28 433		32 640	32 662	32 658
+	28 582	28 577	28 563				
$^2I_{11/2}$	28 770	28 814	28 772	$^2H(1)_{9/2}$	32 689	32 683	-
+	29 008	28 983	-		32 740	32 742	32 744
	29 153	29 106	29 078		-	32 796	-
	-	29 227	29 188				
$^2L_{15/2}$	29 372	29 363	29 334	$^2D(2)_{3/2}$	32 986	-	32 985
	29 501	29 507	29 498		33 141	33 230	33 123
+	-	29 652	-		33 386	-	-
$^4D_{7/2}$	-	29 667	-		33 767	33 806	33 875
+	29 806	-	29 770				
$^2I_{13/2}$	-	29 979	-	$^2D(2)_{5/2}$	33 870	33 855	-
	30 015	30 000	-	$^2H(1)_{11/2}$	33 995	33 969	34 013
	30 127	30 104	-		34 117	34 096	-
	-	30 178	-		34 178	34 137	-
	30 199	30 215	30 248		-	34 208	-
	-	30 268	-		34 262	34 268	34 293
	-	30 298	-		34 311	34 321	-
	30 348	30 345	30 455		34 405	34 400	34 450
	-	30 424	30 395		34 494	-	-
	-	30 467	30 468				
	30 532	30 541	-	$^2F(2)_{5/2}$	37 842	37 886	37 836
	-	30 574	-		38 046	38 163	38 066
	-	30 626	-		38 349	38 333	38 370

levels being drastically different, this level was not taken in the fitting procedure too. This peculiarity has been also reported for other compounds.[37] Due to the complexity of the calculations and the similarities between the experimental energy levels of Nd^{3+} in GdCOB and YCOB (the errors of fitting are larger than these differences), the results of the calculated energy levels are given only for Nd^{3+} in GdCOB.

VI. DISCUSSION

Several characteristics of static crystal field, electron-phonon coupling, nonequivalent centers, and inhomogeneous broadening, revealed by the low-temperature absorption and selective excitation and emission spectra of Nd^{3+} in GdCOB and YCOB as well as crystal field calculations, are analyzed.

(i) *Main Nd^{3+} center crystal field characteristics*. The energy levels of the prevailing Nd^{3+} center (MC) in GdCOB and YCOB associated with the R^{3+} position of C_s symmetry are very similar (Table II), the crystal field splittings being only slightly higher in YCOB. This can be due to smaller lattice constants and higher local stress[38,39] induced by larger Nd^{3+}-Y^{3+} dimensional misfit. The analysis of the energy levels for Nd^{3+} in GdCOB was based on a Hamiltonian consisting of 14 free ion and 14 crystal field parameters for C_s symmetry. The set of obtained parameters gives a good description of experimental data with a root-mean-square de-

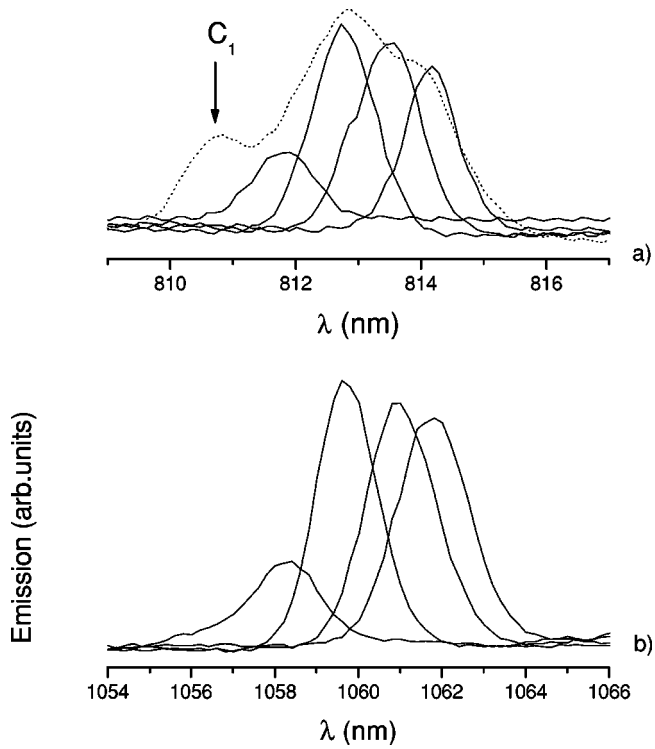

FIG. 7. (a) $^4I_{9/2}(1)\rightarrow F_{5/2}(1)$ excitation spectra monitoring MC $^4F_{3/2}(1)\rightarrow I_{11/2}(1)$ emission. Dotted line: broadband analysis (8.8 nm) centered at 1059 nm. Solid lines from left to right: selective analysis (0.35 nm) at 1058.3, 1059.7, 1061, and 1061.8 nm and (b) corresponding emission spectra.

viation of 17.7 cm^{-1}. The crystal field calculations indicate large second-order crystal field parameters for Nd^{3+} in *R*COB. This is manifested in the large splittings of the $^4F_{3/2}$ level in *R*COB, $\sim$190 cm^{-1}. The Nd^{3+} energy levels in GdCOB and YCOB crystals are similar to those[40,41] of the Nd^{3+} C_2 center in *C*-type Y_2O_3, especially as concerns the splitting of *J* manifolds of the ground term ^4I as shown in Fig. 8, where the Stark levels of the $^4I_{9/2}$ and $^4I_{11/2}$ manifolds are presented. This similarity was found in other isolated transitions; thus, the splitting of the $^4F_{3/2}$ level is comparable to that in Y_2O_3 $\sim$196 cm^{-1} and suggests that the crystal field parameters are close in all these compounds. This is the reason behind the use as a starting set of crystal field parameters in the energy level calculations for Nd^{3+}:*R*COB those obtained for rare-earth *C*-type sesquioxides.[40,41] This similarity of the crystal field effects can be associated with the structure of the centers as illustrated in Fig. 1 and Table I, distorted cubes, rather than the frequently used model of octahedral environment.

The barycenter positions of the ^4I_J manifolds of the ground term for *R*COB are energetically close and Y_2O_3, but the situation is different for isolated excited multiplets although the splittings are similar. This difference could be understood in terms of nephelauxetic effect.[42] For the excited states the nephelauxetic effect is depending principally on the Slater-Condon integral F_2. It has been shown[43] that the $Nd^{3+} \rightarrow {}^2P_{1/2}$ energy level is sensitive to lanthanide-ligand distances as well as to the nature of the ligands. According to

TABLE III. Phenomenological free ion and crystal field parameters for Nd^{3+} in $Ca_4GdO(BO_3)_3$, GdCOB.

Free ion		Crystal field	
Parameter	Value[a] (cm^{-1})	Parameter	Value[a] (cm^{-1})
E^0	23 475(1)	B_0^2	−411(22)
E^1	4745(1)	B_2^2	−865(13)
E^2	23(0.02)	B_0^4	−1746(39)
E^3	478(0.1)	B_2^4	−1477(24)
α	22(0.04)	S_2^4	−287(63)
β	−672(4)	B_4^4	1207(49)
γ	[1567.31]	S_4^4	599(48)
T^2	[321.05]	B_0^6	67(49)
T^3	42(3)	B_2^6	284(40)
T^4	85(2)	S_2^6	−303(69)
T^6	−288(6)	B_4^6	960(21)
T^7	336(7)	S_4^6	158(54)
T^8	[390.96]	B_6^6	194(29)
ζ	871(0.7)	S_6^6	−123(36)

[a]The parameter variance is given in parentheses and the parameters in square brackets were not varied. The number of levels in calculation is 95 with the final mean-square deviation of 17.7 cm^{-1} and residue of 21 908 cm^{-1}.

the mean nearest six R^{3+}-O^{2-} distances in GdCOB (2.360 Å) and Y_2O_3 (2.287 Å), the latter compound is more covalent and the shift of the $^2P_{1/2}$ level to lower energy (22912 cm^{-1}) is possible to apprehend.[44,45] It has been outlined[44] that for two different compounds, but with the same coordination polyhedra, $^2P_{1/2}$ positions could be quite different inasmuch as for one of them the polyhedron is more distorted or the nature of the ligands is different.

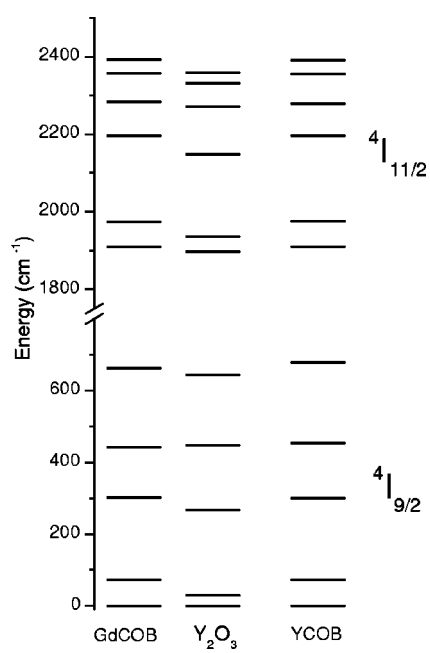

FIG. 8. Comparison between the MC Stark levels of the Nd^{3+} $^4I_{9/2}$, $^4I_{11/2}$ manifolds in GdCOB, Y_2O_3, and YCOB.

Even if the overall crystal field strength for Nd^{3+} in RCOB is comparable with that of Nd^{3+} in YAG, its composition is different (the $^4F_{3/2}$ splitting is $\sim 85\ cm^{-1}$ in YAG). The large splitting $^4F_{3/2}$ for Nd^{3+} in GdCOB, $\sim 193\ cm^{-1}$, has important consequences on the laser properties. In this system, as in many other Nd^{3+} materials, the emission cross section from the upper crystal field component R_2 of the $^4F_{3/2}$ level is larger than that from R_1 and the actual emission wavelength is determined by the product of the emission cross section and the fractional thermal population of the emitting level. Owing to the large splitting of $^4F_{3/2}$, the R_2 is poorly populated at room temperature in GdCOB ($\sim$28%) as compared with YAG ($\sim$40%) and the laser wavelength is determined by the emission from R_1 in the former case, but from R_2 in the latter. However, the heating of the GdCOB crystal during laser emission under an intense pump could modify this fractional thermal population and induce a shift[21,23] of the emission from 1060 nm to 1091 nm. A shift of emission wavelength between levels R_1 and R_2 has been also observed[46] in Nd^{3+}:YAG, but well below room temperature. Such an effect was not mentioned in the case of Nd:YCOB laser experiments,[14,23] although the Nd^{3+} spectral characteristics (Table II) and thermal conductivity cannot explain such differences. Probably the experimental conditions for laser tests were different. No such effects were reported for Nd^{3+} in Y_2O_3 though the $^4F_{3/2}$ level splitting is practically the same to that of GdCOB, but the thermal conductivity is $\sim$6 times larger for Y_2O_3.

(ii) *Electron-phonon coupling effects*. The extended phonon spectrum in RCOB, from 46 cm^{-1} to 1400 cm^{-1}, as shown by the Raman[29,30] or IR (Refs. 7 and 30) data, determines several effects of the electron-phonon interaction for Nd^{3+} in RCOB: strong nonradiative deexcitation[7] (the measured emission lifetime of the metastable $^4F_{3/2}$ level for low concentrations at 300 K is 98 μs for Nd^{3+} in GdCOB compared to estimated radiative lifetime of 659μs), vibronic sidebands, and homogeneous broadening of many zero-phonon lines.

The vibronic sidebands are observed at low temperatures in many transitions; they have comparable intensities with zero-phonon lines in $^4I_{9/2}\rightarrow(^4G_{5/2},{}^2G_{7/2})$, $(^4G_{7/2},{}^2K_{13/2},{}^4G_{9/2})$, and $(^2G(1)_{9/2},{}^2D(1)_{3/2},{}^4G_{11/2},{}^2K_{15/2})$ transitions. Since the phonons in RCOB are both IR and Raman active, a Van Vleck mechanism could be essential in the phonon sideband intensity. Many zero-phonon lines are homogeneously broadened. Due to the complexity of the spectra, our analysis of the broadening is restricted to 10 K; here, the broadening is dominated by one-phonon emission processes and a full width at half maximum (FWHM) up to 50 cm^{-1} was measured. Practically all broadened lines could be connected with phonons present in the Raman spectra. Due to the large phonon frequencies in this crystal, homogeneous broadening by one-phonon emission is observed even in some (1)$\rightarrow$(1) transitions, such as $^4I_{9/2}(1)\rightarrow{}^4G_{5/2}(1)$. However, unlike the Nd^{3+} in YAG,[31] no such broadening process is possible for the $^4I_{9/2}(1)\rightarrow{}^4F_{5/2}(1)$ line in RCOB, an important band for diode pumping. The analysis of the homogeneous broadenings at 10 K brings new arguments of the essential role of optical phonons in the homogeneous line broadening for rare-earth ions in crystals.[46,31]

(iii) *Nonequivalent sites and inhomogeneous broadening*. Nd^{3+} concentration dependence, spectral characteristics, and emission kinetics were followed to elucidate the nature of the three minority C_i centers. The satellite structure is dependent on the transition, and shifts as large as 46 cm^{-1} were measured. In some transitions the spectra are similar in GdCOB and YCOB, but in others significant differences are observed as, for instance, in the $^4I_{9/2}(1)\rightarrow{}^2P_{1/2}$ transition (Fig. 4). Unfortunately we were not able to detect $^2P_{1/2}$ emission, probably due to strong nonradiative deexcitation. The same structure was observed for Nd^{3+}:YCOB samples grown in iridium crucibles and inert atmosphere and in platinum in air. The relative intensity of the $C_{2,3}$ satellites to the total intensity represents about 3%–4% and is almost independent of Nd^{3+} concentration. If the oscillator strengths differences for transitions of the MC and $C_{2,3}$ centers are small, the relative intensity percentage represents an approximately Nd^{3+} relative concentration in perturbed sites. The similarity of $C_{2,3}$ spectra and their resemblance to the MC (Fig. 6), including the lifetimes, leads to the conclusion that they correspond to Nd^{3+} in R^{3+} perturbed positions, the perturbation being connected to some intrinsic lattice defects. The fairly large spectral shifts from MC lines (30–46 cm^{-1}) suggest that the nature of the crystal field perturbation is rather electrical (difference of electric charge) than dimensional (ionic radii differences). Such charged defects could be nonstoichiometric occupancy of some close cationic sites or Gd^{3+} (Y^{3+})$\leftrightarrow Ca^{2+}$ inversion. The estimated degree of disorder in GdCOB is not large and is difficult to estimate by other methods, as shown by the contradictory results[9,12,23] of nonoptical methods, which do not agree with first reports.[1,2] The energy levels of the ^4I term of the C_1 Nd^{3+} center are quite different from the MC and the other perturbed centers (Fig. 6). The lifetimes of C_1 centers are slightly lower in comparison to those of the MC, probably due to the radiative lifetime modifications induced by a different crystal field. The C_1 center could correspond to Nd^{3+} in a Ca^{2+} site with a charge compensation. It represents about 2%–3% of the total Nd^{3+} content.

The Nd^{3+} concentration dependence of intensities and lifetimes for C_i centers is incompatible with a pair model. Due to the differences of the ionic radii between Nd^{3+} and Gd^{3+} or Y^{3+}, one could expect to observe shifted lines (due to stress effects) connected with pairs, at least for near neighbors (at around 3.5 Å). However, a comparison of the shifts for C_i centers with those published for Nd^{3+} pairs in other matrices[39,47,48] suggests that shifts as large as 30–46 cm^{-1} are unlikely for pairs. Therefore, Nd^{3+} pair lines are unsolved and could only contribute to linewidths.

For some Nd^{3+} lines such as those corresponding to $^4I_{9/2}(1)\rightarrow{}^4F_{3/2}(1)$, $^2P_{1/2}$ transitions, the inhomogeneous broadening can be estimated: the homogeneous part in the ground level connected with one-phonon absorption processes is negligible (the first excited Stark levels are around 70 cm^{-1} in both crystals) and Raman processes are expected to be very small[49] while in the excited states the one-phonon

emission processes are not possible. These lines are almost Gaussian; the FWHM of the R_1 line at 10 K in GdCOB increases with Nd^{3+} content from $\sim 6.5\ cm^{-1}$ for 4 at. % to $\sim 9\ cm^{-1}$ for 7 at. % . The Nd^{3+} lines in YCOB are much larger; the same line for 7 at. % Nd in YCOB has the half width of $\sim 14\ cm^{-1}$.

The inhomogeneous broadening is determined by point lattice defects, stresses induced by dimensional misfit, dislocations, ion-ion interactions, etc. As shown previously[38,50,51] the point defects that determine only local strains lead to a Lorentz line shape at low concentrations and Gaussian at large concentrations. An almost Gaussian line shape is induced by charged defects.[38] The charged defects determine random electric fields in the lattice. If the centers are sites without inversion, as in our case, these internal electric fields can determine energy shifts by the Stark effect, the line shape in this case being almost Gaussian.[38] Only small defect concentrations are needed to give large random fields. The variety of broadening mechanisms could be separated into two parts: those characteristic to the lattice and those dependent on the Nd^{3+} concentration. The main intrinsic defects in *R*COB are charged defects of nonstoichiometric or inversion Gd^{3+} $(Y^{3+}) \leftrightarrow Ca^{2+}$ type. If the distribution of such defects is random, nearby ones produce the satellites while the others contribute to broadening. The contribution to broadening introduced by doping can come from Nd^{3+} and Gd^{3+} or Y^{3+} ionic radii misfits, Nd^{3+} in Ca^{2+} sites—a charge defect, unsolved pairs, or ion-ion magnetic interactions. Thus, it is difficult to make an estimation of the contribution of various mechanisms leading to broadening.

The lines of Nd^{3+} in YCOB are significantly broader than in GdCOB, as illustrated in Fig. 4, and the selective excitation in main lines leads to several emission wavelengths (Fig. 7), a behavior characteristic of crystals with disordered structure. A similar behavior was observed for Yb^{3+} spectra[27] in YCOB. At the present time it is difficult to give a definite explanation of this difference. Partly it could be induced by the larger unsolved shifts for the effects discussed for GdCOB, caused by greater Ca^{2+}-Y^{3+} or Nd^{3+}-Y^{3+} ionic radius misfits. Additional sources of disorder in YCOB could be connected to the presence of more peaks in the (DTA) data cooling curve[28] for YCOB (with only one for GdCOB). The origin of these peaks is still unknown, but it was suggested[28] that they could imply a structural transformation, such as a rotation of the $(BO_3)^{3-}$ group without reorganization of the whole crystal.

In conclusion, new results on Nd^{3+} in GdCOB and YCOB obtained by high-resolution optical spectroscopy at low temperature are reported. Thus, the energy level schemes for prevailing Nd^{3+} centers were obtained and the crystal field calculation gave a set of parameters that describe well the experimental data. The similarity of the crystal field for main centers with that of the Nd^{3+} C_2 center in *C*-type Y_2O_3 crystals, including the large second-order crystal field parameters, was connected to the center structure, distorted cubes rather than octahedra**.** Some laser emission features of Nd^{3+} in GdCOB are connected to the effects of the large second-order crystal field parameters. The spectral characteristics of three minority centers were obtained, the concentration of Nd^{3+} in these positions was estimated, and structural models were proposed. The line shape (Gaussian) and large inhomogeneous broadenings imply that these crystals present a disordered structure. It is suggested that, especially for GdCOB, the degree of disorder is not large, since low-concentration charged defects can induce strong spectral effects. The paper reveals an additional source of disorder in YCOB crystals, manifested mainly in inhomogeneous broadening, but further investigations by alternative methods are necessary to elucidate its origin.

ACKNOWLEDGMENT

A.L. wants to thank CNRS (France) for support.

[1] B. Ilyukhin and B. F. Dzhurinskii, Russ. J. Inorg. Chem. **38**, 847 (1993).
[2] R. Norrestam, M. Nygren, and J. O. Bovin, Chem. Mater. **4**, 738 (1992).
[3] G. J. Dirksen and G. Blasse, J. Alloys Compd. **191**, 121 (1993).
[4] G. Aka, A. Kahn-Harari, D. Vivien, J. M. Benitez, F. Salin, and J. Godard, Eur. J. Solid State Inorg. Chem. **33**, 727 (1996).
[5] M. Iwai, T. Kobayashi, H. Furuya, Y. Mori, and T. Sasaki, Jpn. J. Appl. Phys., Part 2 **36**, L276 (1997).
[6] G. Aka, A. Kahn-Harari, F. Mougel, D. Vivien, F. Salin, P. Coquelin, P. Colin, D. Pelenc, and J. L. Damelet, J. Opt. Soc. Am. B **14**, 2238 (1997).
[7] F. Mougel, G. Aka, A. Kahn-Harari, H. Hubert, J. M. Benitez, and D. Vivien, Opt. Mater. **8**, 161 (1997).
[8] F. Mougel, K. Derdanne, G. Aka, A. Kahn-Harari, and D. Vivien, J. Opt. Soc. Am. B **16**, 164 (1997).
[9] F. Mougel, A. Kahn-Harari, G. Aka, and D. Pelenc, J. Mater. Chem. **8**, 1619 (1998).
[10] D. Vivien, F. Mougel, G. Aka, A. Kahn-Harari, and D. Pelenc, Laser Phys. **8**, 759 (1998).
[11] F. Mougel, F. Auge, G. Aka, A. Kahn-Harari, D. Vivien, F. Balembois, P. Georges, and A. Brun, Appl. Phys. B: Lasers Opt. **67**, 533 (1998).
[12] H. J. Zhang, X. L. Meng, L. Zhu, C. Q. Wang, R. P. Cheng, W. T. Yu, S. J. Zhang, L. K. Sun, Y. T. Chou, W. L. Zhang, H. Wang, and K. S. Wong, Opt. Commun. **160**, 273 (1999).
[13] F. Mougel, G. Aka, A. Kahn-Harari, and D. Vivien, Opt. Mater. **13**, 293 (1999).
[14] Q. Ye, L. Shah, J. M. Eichenholts, D. A. Hammons, R. E. Peale, M. Richardson, and B. T. H. Chai, Opt. Commun. **164**, 33 (1999).
[15] J. M. Eichenholts, D. A. Hammons, L. Shah, Q. Ye, R. E. Peale, M. Richardson, and B. T. H. Chai, Appl. Phys. Lett. **74**, 1954 (1999).
[16] J. Lu, G. Li, S. Zhang, H. Chen, M. Jiang, and Z. Shao, Opt. Commun. **168**, 405 (1999).
[17] C. Q. Wang, Y. T. Chow, W. A. Gambling, S. K. Zhang, Z. X. Cheng, Z. S. Shao, and H. C. Chen, Opt. Commun. **174**, 471

(2000).
[18] G. Aka, F. Mougel, F. Augé, A. Kahn-Harari, D. Vivien, J. M. Benitez, F. Salin, D. Pelenc, F. Balembois, P. Georges, and A. Brun, J. Alloys Compd. **303-304**, 401 (2000).
[19] M. Richardson, D. Hammons, J. Eichenholtz, B. H. T. Chai, Quing Ye, Won Kweon Jang, and L. Shah, J. Korean Phys. Soc. **37**, 633 (2000).
[20] D. A. Hammons, M. Richarson, B. H. T. Chai, A. K. Chin, and R. Jollay, IEEE J. Quantum Electron. **36**, 99 (2000).
[21] G. Lucas-Leclin, F. Auge, F. Balembois, P. Georges, A. Brun, F. Mougel, G. Aka, and D. Vivien, J. Opt. Soc. Am. B **17**, 1526 (2000).
[22] Y. M. Yu (unpublished).
[23] D. Vivien, F. Mougel, F. Augé, G. Aka, A. Kahn-Harari, F. Balembois, J. M. Benitez, G. L-Leclin, P. Georges, A. Brun, P. Aschehoung, J. M. Benitez, N. Le Nain, and M. Jacquet, Opt. Mater. **16**, 313 (2001).
[24] R. Young–Feng, H. Nakao, and T. Sasaki, Chin. Phys. Lett. **17**, 896 (2000).
[25] M. Marezio, Acta Crystallogr. **20**, 723 (1966).
[26] R. D. Shannon, Acta Crystallogr., Sect. A: Cryst. Phys., Diffr., Theor. Gen. Crystallogr. **32**, 751 (1976).
[27] A. Lupei, G. Aka, E. Antic-Fidancev, B. Viana, D. Vivien, and P. Aschehoug, J. Phys.: Condens. Matter **13**, 1107 (2002).
[28] D. Vivien, G. Aka, A. Kahn-Harari, A. Aron, F. Mougel, J. M. Benitez, J. Crystal Growth **237-239**, 621 (2002).
[29] A. Lorriaux-Rubbens, G. Aka, E. Antic-Fidancev, D. A. Keszler, and F. Wallart, J. Raman Spectrosc. **31**, 535 (2000).
[30] G. Dominiak-Dzik, W. Ryba-Romanovski, S. Golab, L. Macalik, J. Hanuza, and A. Pajaczkowska, J. Mol. Struct. **555**, 213 (2000).
[31] A. Lupei, Opt. Mater. **16**, 153 (2001).
[32] B. G. Wybourne, *Spectroscopic Properties of Rare Earths* (Interscience, New York, 1965).
[33] P. Porcher, computer code IMAGE (unpublished).
[34] O. Guillot-Noël, A. Kahn-Harari, B. Viana, D. Vivien, E. Antic-Fidancev, and P. Porcher, J. Phys.: Condens. Matter **10**, 6491 (1998).
[35] E. Antic-Fidancev, J. Aride, M. Lemaitre-Blaise, P. Porcher, and M. Taibi, J. Alloys Compd. **188**, 242 (1992).
[36] M. Faucher and J. Dexpert-Ghys, Phys. Rev. B **24**, 3138 (1981).
[37] M. Faucher, D. Garcia, and P. Porcher, C. R. Acad. Sci., Ser. II: Mec., Phys., Chim., Sci. Terre Univers **308**, 603 (1989).
[38] M. Stoneham, Rev. Mod. Phys. **41**, 82 (1969).
[39] R. L. Cone and R. S. Meltzer, in *Spectroscopy of Solids Containing Rare Earth Ions*, edited by A. A. Kaplyanskii and R. M. Macfarlane (North-Holland, Amsterdam, 1987).
[40] N. C. Chang, J. Chem. Phys. **44**, 4044 (1966).
[41] C. Stone and C. A. Burrus, J. Appl. Phys. **49**, 2281 (1978).
[42] C. K. Jorgensen, Prog. Inorg. Chem. **4**, 73 (1962).
[43] E. Antic-Fidancev, M. Lemaitre-Blaise, and P. Caro, New J. Chem. **11**, 467 (1987).
[44] E. Antic-Fidancev, J. Alloys Compd. **300-301**, 2 (2000).
[45] P. Caro, O. Beaury, and E. Antic, J. Phys. (France) **37**, 671 (1976).
[46] A. A. Kaminskii, *Laser Crystals* (Springer-Verlag, Berlin, 1981).
[47] V. Lupei, A. Lupei, C. Tiseanu, S. Georgescu, and C. Stoicescu, Phys. Rev. B **51**, 8 (1995).
[48] A. Lupei, V. Lupei, and S. Georgescu, J. Phys.: Condens. Matter **4**, L221 (1992).
[49] M. MacFarlane, J. Lumin. **85**, 181 (2000).
[50] D. L. Orth, R. J. Mashl, and J. L. Skinner, J. Phys.: Condens. Matter **5**, 2533 (1993).
[51] L. Rogobete, A. Lupei, A. Petraru, and B. Diaconescu, Proc. SPIE **4430**, 28 (2001).